# Elastohydrodynamic Lubrication of Conformal Bearing Systems

Stephen Boedo
Rochester Institute of Technology

**Abstract**

It is well known that structural elasticity plays a prominent role in the performance of fluid film bearing systems. Previous work in elastohydrodynamic (EHD) bearing lubrication has focused on the development of computational algorithms that are particularly useful for conformal bearing systems subjected to dynamic loading. This paper reports on the means to integrate a mode-based EHD lubrication model with substructuring and superlement capabilities in ANSYS to predict bearing performance (film thickness, film pressure) and structural performance (distributed stresses) for dynamically loaded journal bearings. An automotive connecting rod is presented as a case study.

## Introduction

Fluid film conformal bearings are encountered in a wide variety of applications, from automotive engine bearings to artificial hip joints. These bearings are characterized by elastohydrodynamic (EHD) interactions that often produce structural deformations on the order of the lubricant thickness. Further complications include the presence of cavitation, dynamic loading, and transient squeeze film effects.

Representation of the fluid medium as a three-dimensional structure is usually not practical for lubrication problems, as the length scale in the cross-film direction is often much smaller than that along the bearing surfaces. To illustrate this further, Figure 1 shows a schematic of a lubricated bearing with bearing surface length scale L and gap thickness h, respectively. For practical problems of interest, the gap h is typically of the order $10^{-3}$L, which would require an enormous number of ANSYS fluid film elements (FLUID141 or FLUID142) to maintain an adequate element aspect ratio. Moreover, with these length scales, it can be shown (References 1 and 2) that the fluid pressure is essentially constant as one traverses the fluid from one surface to the other, again discouraging the need to discretize the fluid in the cross-film direction.

Similar to plate elements, various researchers have constructed finite element formulations of two-dimensional fluid "film" elements by "building-in" the film thickness variation within the element. The result is two-dimensional elements as shown in Figure 1 with nodal pressures and (cross-film averaged) flows as the set of complementary unknowns (References 3 and 4).

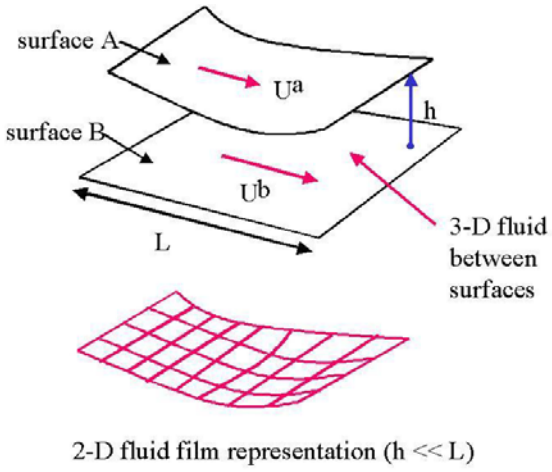


**Figure 1 - Lubricant film model**

This paper discusses the use of ANSYS in analyzing the EHD behavior of fluid film journal bearings under dynamic loading. In particular, this paper will describe the use of ANSYS in the formation of structural stiffness matrices and body force vectors which subsequently serve as input to an EHD software package developed by the author.

## Problem Formulation

Much of what follows is taken from Reference 5 and summarized here for completeness. Figure 2 shows a bearing system comprised of a restrained elastic sleeve and a free rigid journal. An X,Y,Z system frame has its origin at the sleeve center and is fixed to the sleeve. At a given instant in time, external load F (with components defined relative to the X,Y,Z system frame) is applied to the journal and is transmitted to the sleeve via the lubricant film.

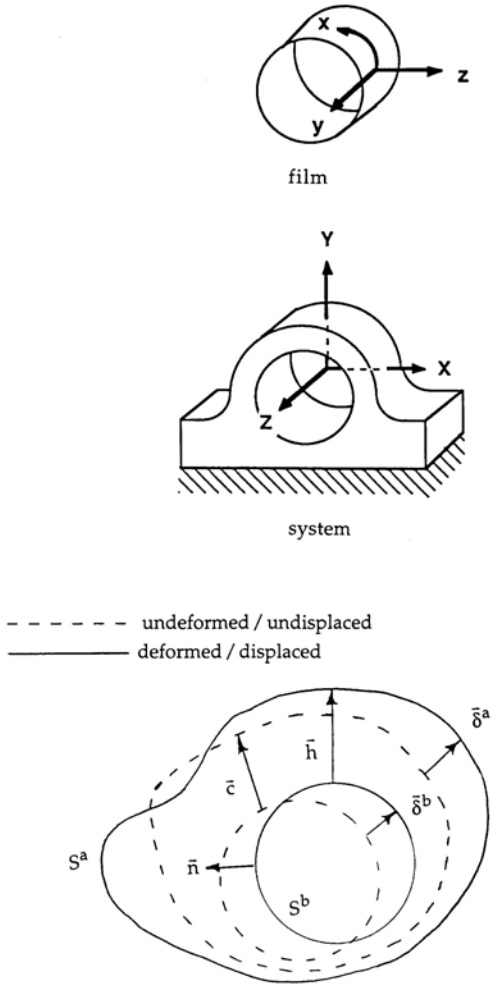


**Figure 2 - Bearing system geometry**

Denoting $S^a$ and $S^b$ as the sleeve and journal surfaces, respectively, Figure 2 defines nominal film thickness h, clearance c, and journal and sleeve surface displacements $\delta^a$ and $\delta^b$, respectively, which are related by the kinematic loop

$$h = c + \delta^a - \delta^b$$

The sleeve structure is represented by a contiguous set of 3-D finite elements, from which one can define a set of master nodal degrees of freedom $\delta^a$ inwardly normal to the surface. Following the usual condensation procedure for finite elements, equilibrium of the sleeve requires

$$\tilde{K}\,\delta^a = r^a + g^a$$

where $\tilde{K}$, $r^a$, and $g^a$ represent the absolute condensed stiffness matrix, normal surface tractions, and condensed body force vector, respectively, acting on the sleeve. Physically, each column of the absolute stiffness matrix can be identified as the nodal normal surface tractions resulting from a unit displacement at a single master node, fixing the other master nodes at zero displacement and ignoring body forces. Physically, the condensed body force vector can be identified as the nodal normal surface tractions

resulting from induced body forces distributed through the structure with all master nodes set to zero displacement.

Figure 3 shows a schematic outline of the EHD lubrication problem described in Reference 5. Stiffness matrix $\tilde{K}$, time histories of external load F, and time histories of condensed body force vector $g^a$ are input to program JBRG (developed by the author) which calculates the transient response of nodal degrees of freedom $\delta^a$ and $\delta^b$ as a linear combination of generalized relative modal displacements $d'$. At each instant in time, film pressures are computed within the JBRG module and are subsequently transferred to the sleeve surface to obtain stress distributions throughout the sleeve structure.

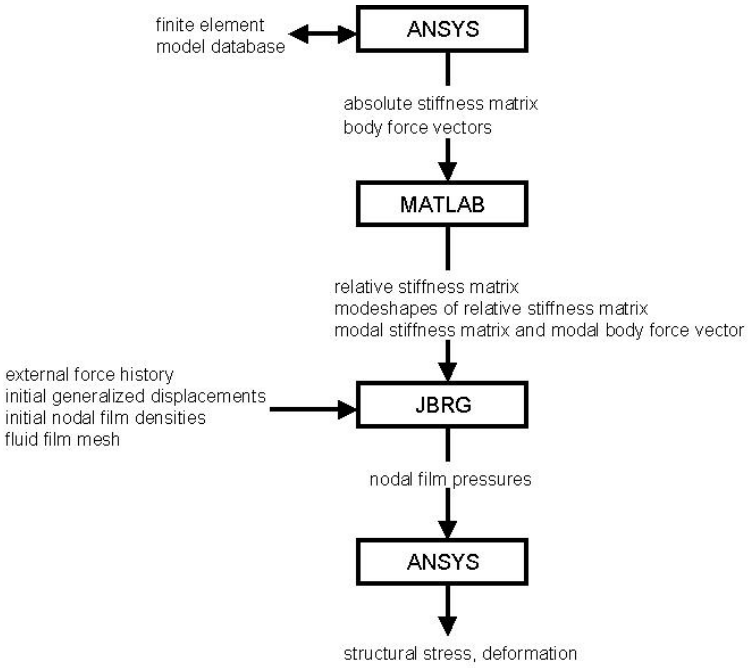


**Figure 3 - Schematic outline of EHD lubrication**

## Application

The modeling of the sleeve structure and determination of the condensed stiffness matrix, body force vector, and stress distributions all employ various modeling and analysis features of ANSYS, and they are best illustrated through the following example.

Figure 4 shows a finite element model representation of an automotive connecting rod constructed from 10-node isoparametric tetrahedral elements (SOLID92), with the intention of assessing the EHD performance of the big-end bearing. The X,Y,Z global Cartesian frame is coincident with the system X,Y,Z frame, both attached to the big-end sleeve center. Nodes on the small-end bearing surface are restrained from radial deflection, and one node on the same surface is restrained from tangential motion to prevent rigid body motion. The half-model assumption requires symmetry displacement boundary conditions invoked along the plane Z = 0. Dimensional specifications are listed in Table 1 as taken from Reference 6.

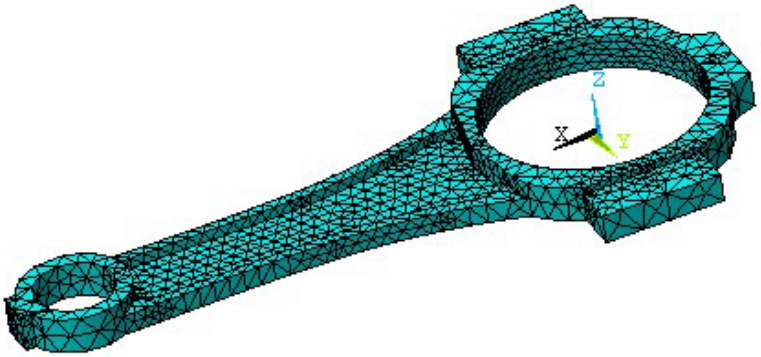


**Figure 4 - Connecting rod finite element model**

Construction of the stiffness matrix requires use of the substructuring analysis option (ANTYPE,SUBSTR) with the stiffness matrix output flag set (SEOPT,,,1). Master nodal degrees of freedom along the inward sleeve surface normals (or radial direction) are defined by first rotating the nodes into the global cylindrical reference frame using CSYS and NROTAT. Prior to invoking the SOLVE command, output is redirected to a file whereupon the stiffness matrix is stored in ASCII format. During this solution run, body forces are suppressed by setting element material density to zero.

Computation of external load components in the X,Y,Z frame are based on consideration of the connecting rod moving with respect to the X', Y', Z' (inertial) block coordinate frame as shown in Figure 5. External load calculations assume a composite crankshaft-connecting rod-piston rigid body mechanism connected with and supported by zero-clearance pin jointed bearings. Figure 6 shows time histories of half-model external components based on engine specifications and cylinder pressure history listed in Table 1. Assuming constant crankshaft angular velocity $\omega = d\theta / dt$, time in this case is conveniently defined as crankangle $\theta$. Details on computing bearing external load can be found in References 6 and 7.

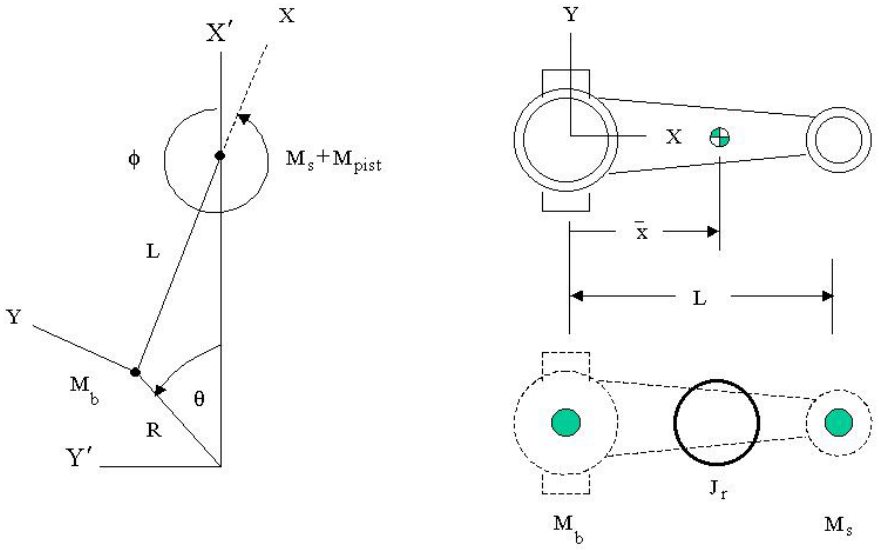


**Figure 5 - Engine mechanism**

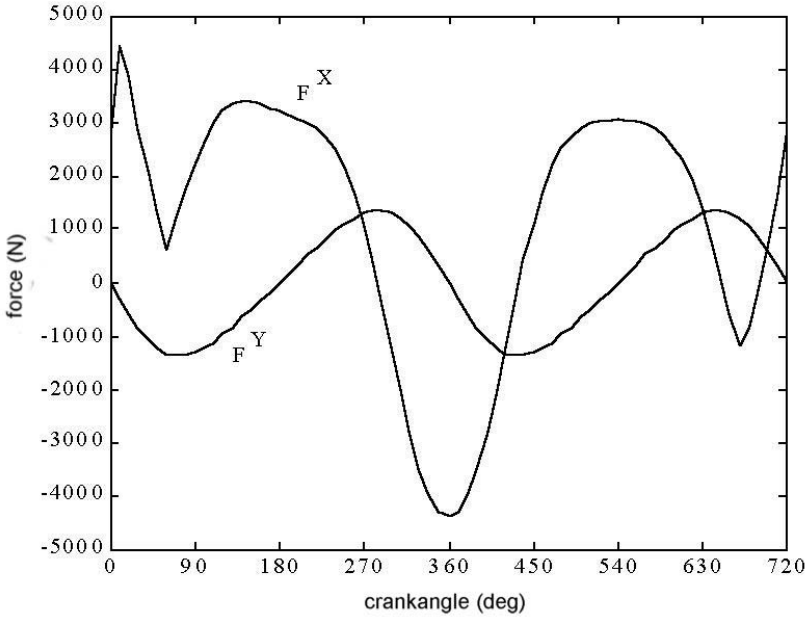


**Figure 6 - External load at 4000 crankshaft rev/min**

Similarly, computation of condensed external body forces $g^a$ requires consideration of a moving connecting rod. Again assuming constant crankshaft angular velocity, the kinematics of the connecting rod can be found from (Reference 7)

$$\theta = \omega t$$

$$\sin\phi = -(R/L)\sin\theta$$

$$\cos\phi = (1 - \sin^2\phi)^{1/2}$$

$$\frac{d\phi}{dt} = \frac{-R\,\omega\cos\theta}{L\cos\phi}$$

$$\frac{d^2\phi}{dt^2} = \frac{R\,\omega^2\sin\theta + L\,(d\phi/dt)^2\sin\phi}{L\cos\phi}$$

Defining a vector from the origin of the X,Y,Z frame to the X',Y',Z' frame gives

$$s^X = -R\cos\theta\cos\phi - R\sin\theta\sin\phi$$

$$s^Y = +R\cos\theta\sin\phi - R\sin\theta\cos\phi$$

from which body forces are applied to the connecting rod model using the following commands:

CGLOC , $s^X$ , $s^Y$

CGOMGA , 0 , 0 , $\omega$

OMEGA , 0 , 0 , $d\phi / dt$

DOMEGA , 0 , 0 , $d^2\phi / dt^2$

Nodes on the sleeve surface are restrained from motion in the inward normal (radial) direction. Upon solution, the reaction forces at the sleeve nodes resulting from induced body forces form the vector $g^a$ at crankangle $\theta$. This process is repeated at fixed crankangle (time) increments over the engine cycle.

## Table 1. Dimensional specifications

*Connecting rod model specifications*

| | | | |
|---|---|---|---|
| Young's modulus | | 210 | GPa |
| Poisson's ratio | | 0.3 | |
| structural density | | 7900 | $kg/m^3$ |
| connecting rod length | L | 145 | mm (center-to-center) |
| mass | M | 0.2558 | kg (half-model) |
| center of mass | $\bar{x}$ | 37.257 | mm |
| polar moment of inertia | J | $1.323 \times 10^{-3}$ | $kg\text{-}m^2$ (half-model) |
| small end mass | $M_s$ | 0.0657 | kg (half-model) |
| big end mass | $M_b$ | 0.1901 | kg (half-model) |
| residual inertia | $J_r$ | $-5.862 \times 10^{-5}$ | $kg\text{-}m^2$ (half-model) |

*Bearing specifications*

| | | |
|---|---|---|
| bearing diameter | 60 | mm |
| bearing length | 10 | mm (half-model) |
| radial clearance | 20 | μm |
| groove width | 1 | mm (half-model) |
| surface roughness | 0 | μm |
| liquid viscosity | 7 | mPa-s |
| liquid density | 850 | $kg/m^3$ |
| supply pressure | 400 | kPa (gage) |
| ambient pressure | 0 | kPa (gage) |
| cavitation pressure | 0 | kPa (gage) |

*Engine specifications*

| | | | |
|---|---|---|---|
| piston mass | $M_{pist}$ | 0.250 | kg (half-model) |
| crank radius | R | 42.5 | mm |
| cylinder area | $A_{cyl}$ | 1290 | $mm^2$ (half-model) |
| crankshaft speed | $\omega$ | $4000(2\pi/60)$ | rad/s |

*Cylinder pressure history*

| crankangle $\theta$ (deg) | cylinder pressure $P_{cyl}$ (kPa) |
|---|---|
| 0 | 5600 |
| 12 | 7000 |
| 60 | 1400 |
| 96 | 700 |
| 144 | 350 |
| 204 | 0 |
| 600 | 0 |
| 648 | 350 |
| 672 | 700 |
| 720 | 5600 |

## Results

The stiffness and body force vectors are input into the JBRG program, and time histories of nodal film pressure, nodal film thickness, and nodal sleeve deformations are output at specified crankangle increments over the complete engine cycle. Lubricant film boundary conditions assume fixed supply pressure within a circumferential groove along the bearing midplane and ambient pressures at the bearing ends. Given a set of nodal film pressures p computed at a specified crankangle, nodal film surface forces acting normal (or radial) to the bearing sleeve are found from

$$r^a = A\,p$$

where A is the area matrix of the bearing sleeve surface. These nodal film surface forces, along with distributed body forces, are applied to the *entire* connecting rod half-model of Figure 4 to obtain nodal displacements and element stresses. Computational details can be found in Reference 6.

Figures 7 and 8 show the influence of body forces on von Mises stress distributions at an engine crankangle of 373 degrees, which is the time corresponding to peak film pressures encountered over the engine cycle. In both cases, nodal film pressures distrubutions calculated by the JBRG program are transferred back to the complete ANSYS model. It is important to observe that, even at 4000 rev/min crankshaft speed, body forces significantly influence the stress distributions throughout the connecting rod, while the neglect of body forces induces artificial bending and thus significantly higher stresses.

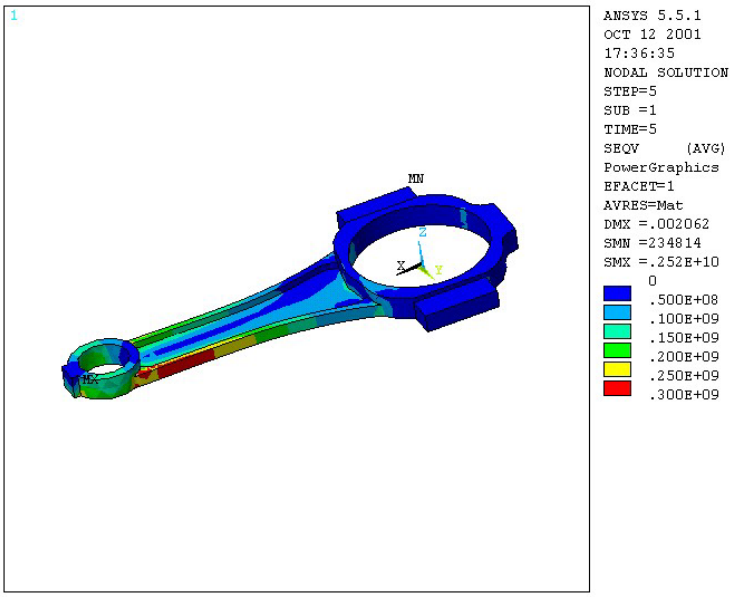


**Figure 7 - Von Mises stress without body forces**

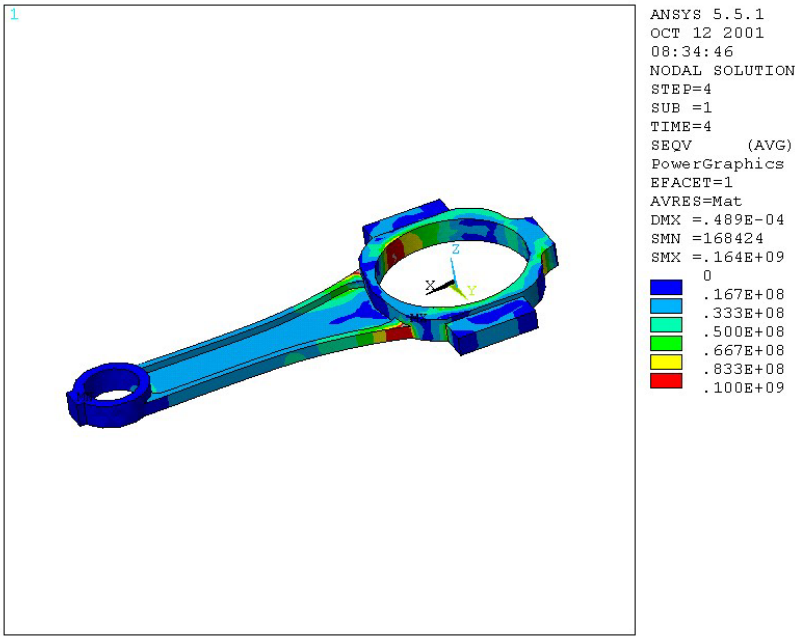


**Figure 8 - Von Mises stress including body forces**

Figure 9 shows contours of instantaneous crankshaft deformation magnitude USUM at an engine crankangle of 373 degrees arising from coupled film pressures and distributed body forces. The maximum observed displacement of approximately 49 μm is more than twice the specified radial clearance of 20 μm, which is quite typical of connecting rod behavior. Such relatively large surface deformations discourage the use of often-employed rigid surface assumptions in characterizing bearing performance.

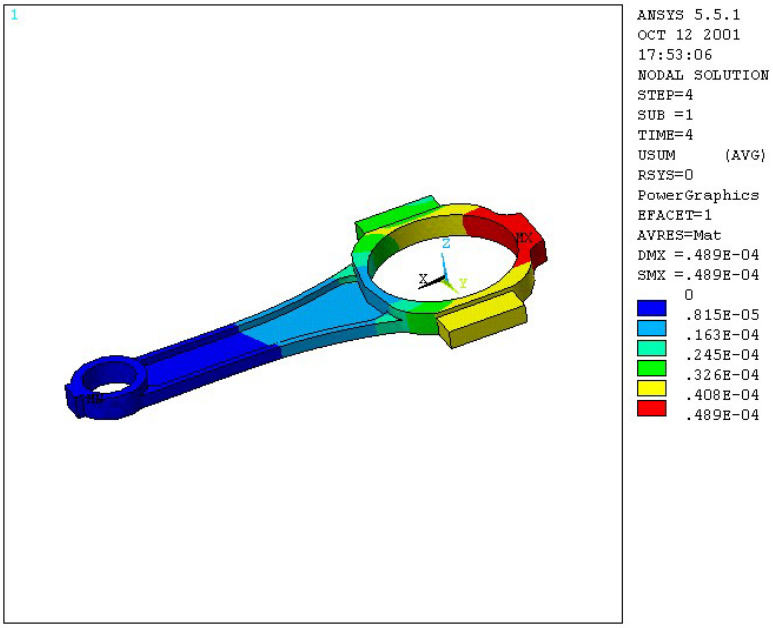


**Figure 9 - Connecting rod deformation**

## Conclusions

This paper has outlined the use of ANSYS in solving problems involving elastohydrodynamic lubrication. Particular emphasis has been focused on the development of body forces, substructuring capablities, and subsequent computation of distributed stresses and deformations arising from from lubricant pressures and body forces. Note that no effort has been made in comparing the lubricant-based stress distributions presented in this paper with those obtained using ANSYS 3-D contact elements, as the boundary conditions are quite different in both cases. For the lubricant film case, relatively small supply and ambient pressures are explicitly applied to the bearing edges, while in the lubricant-free case, relatively large stress concentrations from journal to sleeve line contact are expected along the bearing edges (Reference 8).

### *References*


1) Fantino, B., Godet, M., and Frene J., "Reynolds Equation in Viscous Film Theory," *ASME Journal of Lubrication Technology*, vol. 94, 1972, pp. 287-288.

2) Booker, J.F., "Basic Equations for Fluid Films with Variable Properties," *ASME Journal of Tribology*, vol. 111, 1989, pp. 475-483.

3) Booker, J.F., and Huebner , K.H., "Application of Finite Elements to Lubrication: An Engineering Approach," *ASME Journal of Lubrication Technology*, vol. 94, 1972, p. 313.

4) LaBouff, G.A., and Booker, J.F., "Dynamically Loaded Journal Bearings: A Finite Element Treatment for Rigid and Elastic Surfaces," *ASME Journal of Tribology*, vol. 107, 1985, pp. 505-515.

5) Boedo, S., and Booker, J.F., "Surface Roughness and Structural Inertia in a Mode-Based Mass-Conserving Elastohydrodynamic Lubrication Model," *ASME Journal of Tribology*, vol. 119, 1997, pp. 449-455.

6) Boedo, S., and Booker, J.F., “Finite Element Analysis of Elastic Engine Bearing Lubrication: Application,” *Revue Européenne des Éléments Finis*, in press.

7) Boedo, S., "A Mass-Conserving, Modal-Based Elastohydrodynamic Lubrication Model: Effects of Structural Body Forces, Surface Roughness, and Mode Stiffness Variation," Ph.D. Dissertation, 1995, Cornell University, Ithaca, NY.

8) Harris, T.A., *Rolling Bearing Analysis*, 3rd edition, 1991, John Wiley and Sons, Inc., New York, NY.